

# Disorder-induced magnetooscillations in bilayer graphene at high bias

V. V. Mkhitarian and M. E. Raikh

Department of Physics, University of Utah, Salt Lake City, UT 84112, USA

Energy spectrum of biased bilayer graphene near the bottom has a "Mexican-hat"-like shape. For the Fermi level within the Mexican hat we predict that, apart from conventional magnetooscillations which vanish with temperature, there are additional magnetooscillations which are weakly sensitive to temperature. These oscillations are also insensitive to a long-range disorder. Their period in magnetic field scales with bias,  $V$ , as  $V^2$ . The origin of these oscillations is the disorder-induced scattering between electron-like and hole-like Fermi-surfaces, specific for Mexican hat.

PACS numbers: 73.21.Ac, 73.20.At, 73.43.Qt, 71.55.Jv

*Introduction.* Numerous experimental studies of electronic properties of bilayer graphene were recently reported in the literature [1–15]. From prospective of potential applications, the appeal of bilayer graphene is that a gap can be opened and tuned by the gate voltage [6–15]. Using the dual (top and back) gated structures allows to control both the gap and the carrier density independently [11–15]. For these structures, opening of a gap was demonstrated in temperature [11] and bias [11, 12] dependence of resistivity, in bias dependence of capacitance [14, 15], as well as in strong-field magnetotransport [13]. Measurements in magnetic field reported in the literature focused either on weak-field ( $B \sim 0.1$  T) domain in order to reveal weak localization [2] and universal conductance fluctuations [10], or quantizing ( $B \sim 10$  T) fields [4, 7, 10, 13, 14]. At intermediate fields,  $B \sim 1$  T, transport and capacitance are determined by electron states near the band-edge, Fig. 1. As follows from tight-binding calculation by McCann and Fal'ko [16], the spectrum near the band-edge has a form of "Mexican hat" with minimum at

$$p_0 = \frac{Vt}{v\sqrt{2(V^2 + t^2)}}, \quad (1)$$

where  $v = 8 \times 10^7$  cm/s is the band velocity,  $t$  is the interlayer hopping and  $V$  is the bias. The minimum has a depth,

$$\varepsilon_m = \frac{V}{2} \left( 1 - \frac{t}{\sqrt{V^2 + t^2}} \right). \quad (2)$$

The "capacity" of the minimum for  $t = 0.4$  eV and  $V = 100$  mV is  $n = p_0^2/(\pi\hbar^2) = 0.54 \times 10^{12}$  cm $^{-2}$ . This density is comparable to the densities in experiment [14], but the gap in this experiment was as small as 26 meV. In experiment [15] the gap was wider,  $\approx 100$  meV, but the density was higher,  $\sim 1.5 \times 10^{13}$  cm $^{-2}$ . In both experiments, the Fermi energy exceeded  $\varepsilon_m$ . Upon increasing the bias from  $V = 100$  mV to  $V = 250$  mV, as in experiment [12], the capacity increases by a factor 4.8. This suggests that in the situation Fig. 1, when all electrons reside in is feasible.

In the present paper we demonstrate that, in the regime Fig. 1, when the Fermi energy is smaller than

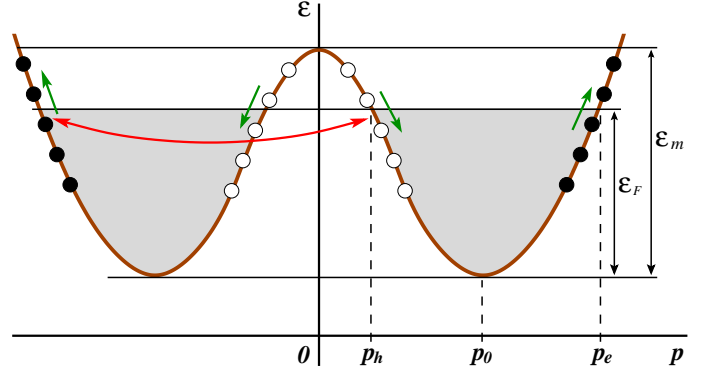


FIG. 1: Energy spectrum of a biased bilayer graphene near the bottom of conduction band. Two Fermi circles, electron-like and hole-like, have radii  $p_e$  and  $p_h$ , respectively. Black dots are electron-like Landau levels. White dots are hole-like Landau levels. Red arrows illustrate scattering process giving rise to additional oscillations. Green arrows illustrate that energies of electron-like Landau levels, Eq. (8), grow with number, while energies of hole-like Landau levels fall off with number.

$\varepsilon_m$ , the behavior of magnetocapacitance,  $\delta C(B)/C^2$ , and magnetoresistance,  $\delta R(B)/R$ , exhibits oscillations, which are additional to conventional magnetooscillations related to the Landau levels. They behave as

$$\frac{\delta C}{C^2} \propto \frac{\delta R}{R} \propto \cos[2\pi p_0^2(V)\lambda^2], \quad (3)$$

where  $\lambda = \sqrt{\hbar c/(eB)}$  is the magnetic length and  $p_0$  is the minimum position of the spectrum, given by Eq. (1). The remarkable feature of the oscillations Eq. (3) is that their period does not contain the Fermi energy,  $\varepsilon_F$ . This suggests that they are not smeared upon increasing temperature, while conventional oscillations are suppressed as  $\exp(-2\pi^2 T/\hbar\omega_c)$ . For the same reason, additional oscillations Eq. (3), unlike conventional magnetooscillations, are insensitive to the random density variations caused by long-range disorder. On the other hand, oscillations Eq. (3) are *disorder-induced*, since it is scattering by short-range disorder which causes the term Eq. (3) in the response functions.

The origin of additional oscillations lies in the fact that, for  $\varepsilon_F < \varepsilon_m$ , the Fermi surface consists of two circles with radii,  $p_e(\varepsilon_F)$  and  $p_h(\varepsilon_F)$ , Fig. 1. Magnetooscillations corresponding to these circles are  $\cos(\pi p_e^2 \lambda^2)$  and  $\cos(\pi p_h^2 \lambda^2)$ , respectively. Due to disorder scattering between the two Fermi circles, magnetocapacitance and magnetoresistance will also contain a product,

$$\begin{aligned} \cos(\pi p_e^2 \lambda^2) \cos(\pi p_h^2 \lambda^2) &= \frac{1}{2} \cos(\pi [p_e^2 - p_h^2] \lambda^2) \\ &+ \frac{1}{2} \cos(\pi [p_e^2 + p_h^2] \lambda^2). \end{aligned} \quad (4)$$

Our prime observation is that  $\varepsilon_F$  drops out of the second term. Indeed, the spectrum of bilayer graphene has a form

$$\varepsilon^2(p) = \frac{V^2}{4} \left(1 - 2\frac{v^2 p^2}{t^2}\right)^2 + \frac{v^4 p^4}{t^2}, \quad (5)$$

so that

$$\begin{aligned} p_e^2 &= p_0^2 + \frac{p_0 t}{vV} \sqrt{2\varepsilon_F(\varepsilon_F + \sqrt{2}vp_0)}, \\ p_h^2 &= p_0^2 - \frac{p_0 t}{vV} \sqrt{2\varepsilon_F(\varepsilon_F + \sqrt{2}vp_0)} \end{aligned} \quad (6)$$

We see that relation  $p_e^2 + p_h^2 = 2p_0^2$  holds for arbitrary  $\varepsilon_F < \varepsilon_m$ . In the remainder of the paper we give a derivation of Eq. (3) with a prefactor and briefly discuss the limit of strong magnetic fields, where the Hall quantization becomes important.

*Density of states.* We start from zero magnetic field. Spectrum Eq. (5) is a result of diagonalization of the  $2 \times 2$  matrix Hamiltonian

$$\mathcal{H} = \begin{pmatrix} \frac{V}{2} \left(1 - 2\frac{v^2 p^2}{t^2}\right) & -\frac{v^2(p_x + ip_y)^2}{t} \\ -\frac{v^2(p_x - ip_y)^2}{t} & -\frac{V}{2} \left(1 - 2\frac{v^2 p^2}{t^2}\right) \end{pmatrix}. \quad (7)$$

It is convenient to find the Landau level spectrum of Eq. (7) using the gauge,  $\mathbf{A} = (0, Bx)$ , in which eigenfunctions of the conventional quadratic spectrum are  $e^{ip_y y} \phi_n(x)$ , with  $\phi_n(x)$  being the eigenfunctions of 1D harmonic oscillator. In this basis, the spectrum for  $n \geq 2$  is

$$\begin{aligned} \varepsilon_n &= -\frac{V}{2t} \hbar \Omega_c \\ &\pm \sqrt{V^2 \left(\frac{1}{2} - \frac{2n-1}{2t} \hbar \Omega_c\right)^2 + (\hbar \Omega_c)^2 n(n-1)} \end{aligned} \quad (8)$$

with  $\Omega_c = 2\hbar v^2/(t\lambda^2)$ , while eigenfunctions are given by

$$\Phi_{n,p_y}(\mathbf{r}) = \frac{e^{ip_y y}}{\sqrt{1+d_n^2}} \begin{pmatrix} \phi_n(x - p_y \lambda^2) \\ d_n \phi_{n-2}(x - p_y \lambda^2) \end{pmatrix}, \quad (9)$$

where

$$d_n = \frac{\varepsilon_n - V \left(\frac{1}{2} - n \frac{\hbar \Omega_c}{t}\right)}{\hbar \Omega_c \sqrt{n(n-1)}}. \quad (10)$$

Spacings between the electron-like and hole-like Landau levels at the Fermi energy are the same,

$$\begin{aligned} \frac{\hbar^2}{\lambda^2} \left| \frac{\partial \varepsilon}{\partial p^2} \right|_{p=p_e} &= \frac{\hbar^2}{\lambda^2} \left| \frac{\partial \varepsilon}{\partial p^2} \right|_{p=p_h} \\ &= \frac{\hbar^2}{\lambda^2} \frac{vV}{2p_0 t} \frac{\sqrt{\varepsilon_F(\varepsilon_F + \sqrt{2}vp_0)}}{\varepsilon_F + vp_0/\sqrt{2}} = \hbar \omega_c. \end{aligned} \quad (11)$$

In the presence of disorder,  $U(\mathbf{r})$ , imaginary part of the self-energy,  $\Sigma_n(E)$ , is determined by level numbers,  $n$ , for which  $\varepsilon_n$  is close to  $E$ . At the same time, the  $n$ -dependence of  $\Sigma_n(E)$  is weak. In our case, however, the equation  $\varepsilon_n = E$  has *two* different solutions:  $2n_e \simeq p_e^2 \lambda^2$  and  $2n_h \simeq p_h^2 \lambda^2$ . Correspondingly, one should consider two different self-energies,  $\Sigma_{n_e} \equiv \Sigma_e$  and  $\Sigma_{n_h} \equiv \Sigma_h$ . As demonstrated in [19], short-range disorder (with correlation length smaller than  $\lambda$ ) insures the applicability of the self-consistent Born approximation (SCBA), which in our case becomes a system

$$\frac{\Sigma_e(E)}{\Gamma^2} = \sum_{n,e} \frac{\alpha_{ee}}{E - \varepsilon_n - \Sigma_e(E)} + \sum_{n,h} \frac{\alpha_{eh}}{E - \varepsilon_n - \Sigma_h(E)}, \quad (12)$$

$$\frac{\Sigma_h(E)}{\Gamma^2} = \sum_{n,h} \frac{\alpha_{hh}}{E - \varepsilon_n - \Sigma_h(E)} + \sum_{n,e} \frac{\alpha_{he}}{E - \varepsilon_n - \Sigma_e(E)}, \quad (13)$$

where subscript  $(n, e)$  or  $(n, h)$  indicates that the summation is performed for  $n$  close to  $n_e$  or  $n_h$ , respectively. Coefficients

$$\alpha_{ee} = \frac{1 + |d_{n_e}|^4}{(1 + |d_{n_e}|^2)^2}, \quad \alpha_{eh} = \frac{1 + |d_{n_e}|^2 |d_{n_h}|^2}{(1 + |d_{n_e}|^2)(1 + |d_{n_h}|^2)} \quad (14)$$

do not contain numbers of Landau levels, since they are taken at  $n = n_e$  and  $n = n_h$ , correspondingly. Explicit expressions for  $d_{n_e}$  and  $d_{n_h}$  as a function of the Fermi energy are the following

$$d_{n_e} = \frac{V}{t} + \frac{t(\varepsilon_F - \varepsilon_m)}{v^2 p_e^2}, \quad d_{n_h} = \frac{V}{t} + \frac{t(\varepsilon_F - \varepsilon_m)}{v^2 p_h^2}, \quad (15)$$

where  $\varepsilon_m$  is given by Eq. (2), and  $p_e, p_h$  are given by Eq. (6). Coefficients  $\alpha_{hh}$  and  $\alpha_{he}$  in Eq. (13) are given by Eq. (14) with replacement,  $e \rightleftharpoons h$ . Coefficient  $\Gamma^2$  describes the strength of the disorder potential,  $\Gamma^2 = \int d^2 \mathbf{r} \langle U(0)U(\mathbf{r}) \rangle / (2\pi\lambda^2)$ . Second terms in Eqs. (12), (13) describe contributions from disorder-induced mixing of electron-like and hole-like Landau levels.

Applying the Poisson summation formula to the sums in Eqs. (12), (13), we get the following equations for the imaginary parts  $\text{Im}\Sigma = \Sigma''$ ,

$$\begin{aligned} \Sigma''_e(\varepsilon_F) &= \frac{\hbar}{2\tau_e} + \frac{2\pi\Gamma^2}{\hbar\omega_c} \alpha_{ee} \exp\left[-\frac{2\pi\Sigma''_e}{\hbar\omega_c}\right] \cos(\pi p_e^2 \lambda^2) \\ &+ \frac{2\pi\Gamma^2}{\hbar\omega_c} \alpha_{eh} \exp\left[-\frac{2\pi\Sigma''_h}{\hbar\omega_c}\right] \cos(\pi p_h^2 \lambda^2), \end{aligned} \quad (16)$$

$$\begin{aligned} \Sigma''_h(\varepsilon_F) &= \frac{\hbar}{2\tau_h} + \frac{2\pi\Gamma^2}{\hbar\omega_c} \alpha_{hh} \exp\left[-\frac{2\pi\Sigma''_h}{\hbar\omega_c}\right] \cos(\pi p_h^2 \lambda^2) \\ &+ \frac{2\pi\Gamma^2}{\hbar\omega_c} \alpha_{he} \exp\left[-\frac{2\pi\Sigma''_e}{\hbar\omega_c}\right] \cos(\pi p_e^2 \lambda^2), \end{aligned} \quad (17)$$

where  $\tau_e$  and  $\tau_h$  are the *full* scattering times from the states  $p_e$  and  $p_h$  in a zero magnetic field,

$$\frac{\hbar}{\tau_e} = \frac{2\pi\Gamma^2}{\hbar\omega_c} (\alpha_{ee} + \alpha_{eh}), \quad \frac{\hbar}{\tau_h} = \frac{2\pi\Gamma^2}{\hbar\omega_c} (\alpha_{hh} + \alpha_{he}). \quad (18)$$

We note that magnetic-field dependence drops out from the ratio  $\Gamma^2/(\hbar\omega_c)$ . Concerning the energy dependence of  $\tau_e$  and  $\tau_h$ , it follows from Eq. (11) that near the bottom of Mexican hat,  $\varepsilon_F \ll \varepsilon_m$ , we have  $\tau_e, \tau_h \sim \sqrt{\varepsilon_F}$ , which reflects the 1D character of the bear density of states [20]. Iterating Eqs. (16), (17), we obtain a contribution to the density of states of the form

$$\delta g(B) = G_0 \exp\left[-\frac{\pi}{\omega_c \tau_e} - \frac{\pi}{\omega_c \tau_h}\right] \cos(2\pi p_0^2 \lambda^2), \quad (19)$$

which coincides with additional oscillations Eq. (3) stated in the Introduction. Prefactor  $G_0$  is given by  $G_0 = 4\pi\Gamma^2 \alpha_{eh} / [(\hbar\omega_c)^3 \lambda^2]$ . Magnetic field dependence of  $G_0$  is  $\propto 1/B$ . Energy dependence of  $G_0$  is plotted in Fig. 2. We see that  $G_0$  diverges in the limit  $\varepsilon_F \rightarrow 0$ . This divergence is also due to the 1D character of the density of states near the bottom of the Mexican hat. As the Fermi level approaches the top of the Mexican hat, the hole contributions in Eqs. (16), (17), and resulting additional oscillations, disappear. At the same time the prefactor  $G_0$  remains finite in the limit  $\varepsilon_F \rightarrow \varepsilon_m$ . Such an abrupt behavior of additional oscillations is a consequence of the fact that the bare density of states experiences a jump at  $\varepsilon_F = \varepsilon_m$ .

*Conductivity* To trace the emergence of the product  $\cos(\pi p_e^2 \lambda^2) \cos(\pi p_h^2 \lambda^2)$  in the conductivity,  $\sigma$ , it is sufficient to set  $\Sigma''_e = \hbar/\tau_e$  and  $\Sigma''_h = \hbar/\tau_h$  in the exponents in Eqs. (16), (17). The SCBA expression for  $\sigma$  in the case of bilayer graphene is the sum of electron-like and hole-like contributions

$$\sigma(E) = \sigma_e(E) + \sigma_h(E), \quad (20)$$

where  $\sigma_e$  can be presented in the form of a sum,

$$\begin{aligned} \sigma_e(E) &= \frac{\hbar e^2}{\pi^2 \lambda^2} \\ &\times \sum_{n,e} \frac{\langle v_x \rangle_{n,n+1}^2 (\Sigma''_e)^2}{\left[ (E - \varepsilon_n)^2 + (\Sigma''_e)^2 \right] \left[ (E - \varepsilon_{n+1})^2 + (\Sigma''_e)^2 \right]}, \end{aligned} \quad (21)$$

and  $\sigma_h$  is given by Eq. (21) with replacement of subindex  $e$  by  $h$ . Matrix element  $\langle v_x \rangle_{n,n+1}$  taken between the states Eq. (9) is

$$\langle v_x \rangle_{n,n+1} = \pm i \lambda \omega_c \frac{\sqrt{n+1} + d_n d_{n+1} \sqrt{n-1}}{\sqrt{2(1+|d_n|^2)(1+|d_{n+1}|^2)}}. \quad (22)$$

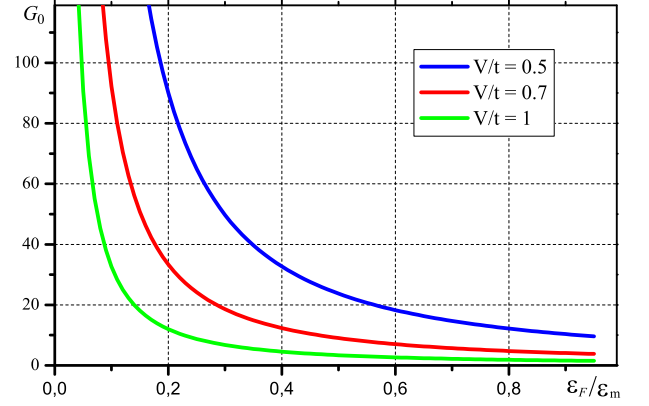


FIG. 2: Prefactor in "magnetocapacitance"  $\delta g(B)$ , Eq. (19), in the units of  $4\pi\Gamma^2 \lambda^4 [2p_0 t / (\hbar^2 v V)]^3$ , is plotted from Eqs. (11), (14), and (15), versus dimensionless ratio  $\varepsilon_F/\varepsilon_m$  for three values of the ratio,  $V/t = 0.5$ ,  $V/t = 0.7$ , and  $V/t = 1$ .

Now we notice that a term proportional to the product of two cosines Eq. (4) follows from  $(\Sigma''_e)^2$  in the numerator of Eq. (21). Indeed, plugging Eq. (16) into the numerator of Eq. (21) and replacing  $(\Sigma''_e)^2$  in denominator with its leading value  $\hbar^2/\tau_e^2$ , we arrive at additional oscillations

$$\frac{\delta \sigma_e}{\sigma_e^0} = \frac{e^2}{2\pi\hbar} \frac{\tau_e^2}{\tau_{ee}\tau_{eh}} \exp\left[-\frac{\pi}{\omega_c \tau_e} - \frac{\pi}{\omega_c \tau_h}\right] \cos(2\pi p_0^2 \lambda^2), \quad (23)$$

where we have introduced the Drude conductivity

$$\sigma_e^0 = \frac{p_e^2 \lambda^2}{2\hbar^2} \frac{\omega_c \tau_e}{1 + \omega_c^2 \tau_e^2}. \quad (24)$$

A more accurate form of  $\delta \sigma_e/\sigma_e^0$  can be found by applying the Poisson summation formula to Eq. (21), which will include corrections to self-energies in the denominator. This transforms Eq. (23) into

$$\begin{aligned} \frac{\delta \sigma_e}{\sigma_e^0} &= \frac{e^2}{2\pi\hbar} \frac{\tau_e^2}{\tau_{ee}\tau_{eh}} \frac{1 - \omega_c^2 \tau_e^2}{1 + \omega_c^2 \tau_e^2} \\ &\times \exp\left[-\frac{\pi}{\omega_c \tau_e} - \frac{\pi}{\omega_c \tau_h}\right] \cos(2\pi p_0^2 \lambda^2), \end{aligned} \quad (25)$$

which differs from Eq. (23) in strong,  $\omega_c \tau_e > 1$ , magnetic fields. For the contribution  $\sigma_h$ , relations Eq. (25) holds with replacement of subindexes  $e \rightleftharpoons h$ .

*Concluding remarks.* (i) Up to now, observing the Mexican hat structure of the spectrum in experiments on bilayer graphene was limited by relatively low mobility,  $\mu \sim 2000 - 3000 \text{ cm}^2/\text{Vs}$ . This corresponds to the energy smearing,  $\hbar/\tau$ , of about  $7 - 10 \text{ meV}$ . In particular, revealing Landau quantization in magnetotransport [1, 7, 10, 13], ac [4], and magnetocapacitance [14, 15] experiments required strong magnetic field,  $B \sim 10 \text{ T}$ . Typical cyclotron quantum for such fields is  $\hbar\omega_c \sim 20 \text{ meV}$ ,

i.e., it is bigger than  $\varepsilon_m \approx 11$  meV for  $V = 0.2$  V. On the other hand, inhomogeneity of local electron density [14] was a significant factor in smearing of magnetooscillations. In this regard, additional oscillations Eq. (3), being insensitive to this inhomogeneity, might be observable even when conventional magnetooscillations are completely washed out. For  $B = 1$  T and same  $V = 0.2$  V condition  $\varepsilon_m > \hbar\omega_c$  is satisfied; for this  $V$ , the product  $p_0^2\lambda^2$  in the argument of Eq. (3) is 38. For such fields, conventional oscillations are suppressed at temperatures as low as  $T = 3$  K, while additional oscillations Eq. (3) remain unaffected. Unlike conventional magnetooscillations [18], they are also insensitive to the lifting of valley degeneracy.

(ii). Our calculation was based on the spectrum Eq. (5); this spectrum is obtained from  $2 \times 2$  Hamiltonian Eq. (7). Analysis of more general  $4 \times 4$  Hamiltonian [16, 17] suggests that the gap can exceed  $t$  while the property,  $p_e^2 + p_h^2 = 2p_0^2$  persists.

(iii). Relevant densities for the additional oscillations are  $\sim 10^{12}$  cm $^{-2}$ . Such densities are high enough for electron-electron interaction-induced spectrum renormalization to be insignificant [22–24]. On the other hand, interactions can scatter electrons between electron-like and hole-like Fermi surfaces. They also induce inelastic lifetime  $\sim \varepsilon_F/T^2$ . This leads to effective suppression of additional oscillations at temperatures above  $T \sim \sqrt{\varepsilon_F\hbar\omega_c} \sim 50$  K.

(iv). To establish a relation between oscillation Eq. (3) and magnetointersubband oscillations in a quantum well with two subbands [21], let us turn to the product Eq. (4) of the oscillating part of the density of states. Magnetointersubband oscillations of Ref. [21] follow from the similar product for different subbands. However, they emerge from the term,  $\cos[\pi(p_e^2 - p_h^2)\lambda^2]$ , of Eq. (4), while oscillations Eq. (3) come from the term  $\cos[\pi(p_e^2 + p_h^2)\lambda^2]$  of Eq. (4). Independence of this term of  $\varepsilon_F$  is specific for bilayer graphene.

(v). In closing, we discuss qualitatively the limit of quantizing magnetic fields. When the Fermi level lies within the Mexican hat, classical trajectories corresponding to electron-like and hole-like states are Larmour circles with *opposite* direction of rotation. Indeed, the equation of motion in momentum space,  $\dot{\mathbf{p}} = \frac{e}{c} \frac{\partial \varepsilon}{\partial \mathbf{p}} \times \mathbf{B}$ , can be presented as

$$\dot{\mathbf{p}} = \frac{e}{c} \left( \frac{vV}{p_0 t} \right)^2 \frac{p^2 - p_0^2}{2\varepsilon} (\mathbf{p} \times \mathbf{B}). \quad (26)$$

With energy and absolute value of momentum conserved by Eq. (26), the only difference between electron-like and hole-like motions comes from the factor,  $(p^2 - p_0^2)$ . Since  $(p_e^2 - p_0^2) = -(p_h^2 - p_0^2)$ , clockwise rotation of electron-like states and anti-clockwise rotation of hole-like states have the same frequency, in agreement with Eq. (11). At the same time, the radii and velocities of their Larmour motions are related as  $p_e/p_h$ .

Opposite directions of rotation for electron-like and hole-like states translate into the opposite signs of drift velocities for corresponding edge states,

$$v_e = \left( \frac{vV}{p_0 t} \right)^2 \frac{p_e^2 - p_0^2}{2\varepsilon} \frac{\sqrt{p_e^2 - p_y^2}}{\pi - \arccos(p_y/p_e)},$$

$$v_h = \left( \frac{vV}{p_0 t} \right)^2 \frac{p_h^2 - p_0^2}{2\varepsilon} \frac{\sqrt{p_h^2 - p_y^2}}{\pi - \arccos(p_y/p_h)}. \quad (27)$$

This, in turn, means that dispersion laws for electron-like and hole-like states *intersect* each other. Previously, Refs. [25, 26] pointed out that opposite dispersion of the edge states from the *same* Landau level can arise from the valley splitting. Combined with the Zeeman splitting, this leads to intersecting edge dispersions for opposite spin directions [25]. We note that in bilayer graphene with the Fermi level within the Mexican hat, crossing of the edge dispersions from *different* Landau levels occurs naturally with the valley degeneracy preserved. For the Fermi level located at the intersection of electron- and hole-dispersion curves, interactions can result in non-chiral Luttinger liquid at the edge. This situation is similar to the quantum Hall line junction considered in Refs. [27, 28]. Unlike Refs. [27, 28], where the disorder results in resonant-tunnelling states between the edges separated by a tunnel barrier, in our case disorder will smear the corresponding Luttinger-liquid anomalies.

- 
- [1] K. S. Novoselov, E. McCann, S. V. Morozov, V. I. Falko, M. I. Katsnelson, U. Zeitler, D. Jiang, F. Schedin, and A. K. Geim, Nat. Phys. **2**, 177 (2006).
  - [2] R. V. Gorbachev, F. V. Tikhonenko, A. S. Mayorov, D. W. Horsell, and A. K. Savchenko, Phys. Rev. Lett. **98**, 176805 (2007).
  - [3] S. V. Morozov, K. S. Novoselov, M. I. Katsnelson, F. Schedin, D. C. Elias, J. A. Jaszczak, and A. K. Geim, Phys. Rev. Lett. **100**, 016602 (2008).
  - [4] E. A. Henriksen, Z. Jiang, L.-C. Tung, M. E. Schwartz, M. Takita, Y.-J. Wang, P. Kim, and H. L. Stormer, Phys. Rev. Lett. **100**, 087403 (2008).
  - [5] J. Yan, E. A. Henriksen, P. Kim, and A. Pinczuk, Phys. Rev. Lett. **101**, 136804 (2008).
  - [6] T. Ohta, A. Bostwick, T. Seyller, K. Horn, and E. Rotenberg, Science **313**, 951 (2006).
  - [7] E. V. Castro, K. S. Novoselov, S. V. Morozov, N. M. R. Peres, J. M. B. Lopes dos Santos, J. Nilsson, F. Guinea, A. K. Geim, and A. H. Castro Neto, Phys. Rev. Lett. **99**, 216802 (2007).
  - [8] L. M. Zhang, Z. Q. Li, D. N. Basov, M. M. Fogler, Z. Hao, and M. C. Martin, Phys. Rev. B **78**, 235408 (2008).
  - [9] Z. Q. Li, E. A. Henriksen, Z. Jiang, Z. Hao, M. C. Martin, P. Kim, H. L. Stormer, and D. N. Basov, Phys. Rev. Lett. **102**, 037403 (2009).
  - [10] Y. Ujiie, S. Motooka, T. Morimoto, N. Aoki, D. K. Ferry, J. P. Bird, and Y. Ochiai, J. Phys.: Condens. Matter **21**, 382202 (2009).

- [11] J. B. Oostinga, H. B. Heersche, X. Liu, A. F. Morpurgo, and L. M. K. Vandersypen, *Nature Mater.* **7**, 151 (2008).
- [12] Y. Zhang, T.-T. Tang, C. Girit, Z. Hao, M. C. Martin, A. Zettl, M. I. F. Crommie, Y. Ron Shen, and F. Wang *Nature* **459**, 820 (2009).
- [13] S. Kim and E. Tutuc, arXiv: 0909.2288.
- [14] E.A. Henriksen and J.P. Eisenstein, arXiv:1004.2543.
- [15] A.F. Young, C.R. Dean, I. Meric, S. Sorgenfrei, H. Ren, K. Watanabe, T. Taniguchi, J. Hone, K.L. Shepard, and P. Kim, arXiv:1004.5556.
- [16] E. McCann and V. I. Fal'ko, *Phys. Rev. Lett.* **96**, 086805 (2006).
- [17] A. H. Castro Neto, F. Guinea, N. M. R. Peres, K. S. Novoselov, and A. K. Geim, *Rev. Mod. Phys.* **81**, 109 (2009).
- [18] M. Nakamura, E. V. Castro, and B. Dóra, *Phys. Rev. Lett.* **103**, 266804 (2009).
- [19] M. E. Raikh and T. V. Shahbazyan, *Phys. Rev. B* **47**, 1522 (1993).
- [20] V. V. Mkhitarian and M. E. Raikh *Phys. Rev. B* **78**, 195409 (2008).
- [21] V. Polyakovskiy, *Fiz. Tekh. Poluprovodn.* **22**, 2230 (1988) [*Sov. Phys. Semicond.* **22**, 1408 (1988)]; M. E. Raikh and T. V. Shahbazyan, *Phys. Rev. B* **49**, 5531 (1994).
- [22] T. Stauber, N. M. R. Peres, F. Guinea, and A. H. Castro Neto, *Phys. Rev. B* **75**, 115425 (2007).
- [23] G. Borghi, M. Polini, R. Asgari, and A. H. MacDonald, arXiv:1005.2156.
- [24] S. Viola Kusminskiy, J. Nilsson, D. K. Campbell, and A. H. Castro Neto, *Phys. Rev. Lett.* **100**, 106805 (2008).
- [25] D. A. Abanin, P. A. Lee, and L. S. Levitov, *Phys. Rev. Lett.* **96**, 176803 (2006).
- [26] L. Brey and H.A. Fertig, *Phys. Rev. B* **73**, 195408 (2006).
- [27] E.-A. Kim and E. Fradkin, *Phys. Rev. B* **67**, 045317 (2003).
- [28] I. Yang, W. Kang, L. N. Pfeiffer, K. W. Baldwin, K. W. West, E.-A. Kim, and E. Fradkin, *Phys. Rev. B* **71**, 113312 (2005).